NANO LETTERS

Letter

pubs.acs.org/NanoLett

Two-Minute Assembly of Pristine Large-Area Graphene Based Films

Jongwon Shim,[†,‡,▽] Je Moon Yun,[†,‡] Taeyeong Yun,[†,‡] Pilnam Kim,[§] Kyung Eun Lee,[†,‡] Won Jun Lee,[†,‡] Ryong Ryoo,[†,∥] David J. Pine,*[,⊥,#] Gi-Ra Yi,*[,#] and Sang Ouk Kim*[,†,‡]

[†]Center for Nanomaterials and Chemical Reactions, Institute for Basic Science (IBS), Daejeon 305-701, Republic of Korea

[‡]Department of Materials Science and Engineering, KAIST, Daejeon 305-701, Republic of Korea

[§]Department of Bio and Brain Engineering, KAIST, Daejeon 305-701, Republic of Korea

[∥]Department of Chemistry, KAIST, Daejeon 305-701, Republic of Korea

[⊥]Department of Physics, New York University, New York, New York 10003, United States

[#]School of Chemical Engineering, Sungkyunkwan University, Suwon 440-746, Republic of Korea

[▽]Advanced Materials Research Team, AMOREPACIFIC R&D Center, Yongin 446-729, Republic of Korea

Supporting Information

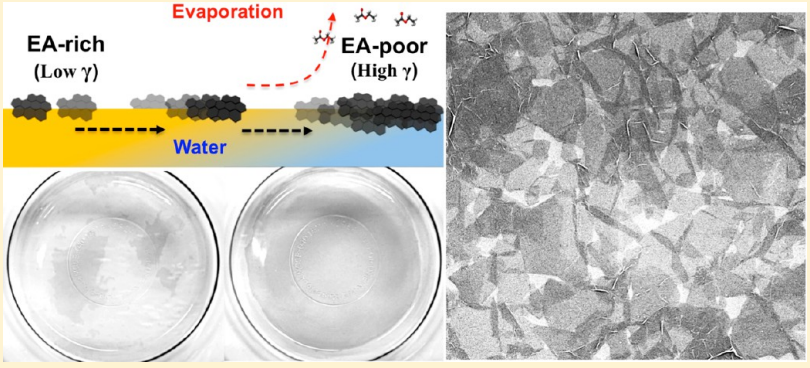

ABSTRACT: We report a remarkably rapid method for assembling pristine graphene platelets into a large area transparent film at a liquid surface. Some 2−3 layer pristine graphene platelets temporally solvated with *N*-methyl-2-pyrrolidone (NMP) are assembled at the surface of a dilute aqueous suspension using an evaporation-driven Rayleigh-Taylor instability and then are driven together by Marangoni forces. The platelets are fixed through physical binding of their edges. Typically, 8-cm-diameter circular graphene films are generated within two minutes. Once formed, the films can be transferred onto various substrates with flat or textured topologies. This interfacial assembly protocol is generally applicable to other nanomaterials, including 0D fullerene and 1D carbon nanotubes, which commonly suffer from limited solution compatibility.

KEYWORDS: *Graphene, interface, assembly, film*

Owing to the inherent two-dimensional nature of graphene, its principal applications are anticipated to be as a macroscopic film or sheet structures.[1−3] Graphene's outstanding material properties, including high electrical/thermal conductivity and superstrong mechanical properties along the two-dimensional graphene plane, can be exploited for diverse applications. Presently, transparent graphene film preparation relies principally on CVD growth from metal catalysts. CVD growth offers high-quality large-area graphene.[4,5] Nevertheless, vacuum processing at high temperature is expensive and requires long batch times. Moreover, film transfer onto desired substrates suffers from hard metal catalyst etching and polymer adhesive residues.[6]

Solution processing of pristine graphene based films has great potential for the cost-effective production of surface coating,[7,8] composites,[9,10] flexible electrodes,[11,12] sensors,[13,14] mechanical resonators,[15] separation membranes,[16] and so on. However, the low solution compatibility of pristine graphene, particularly in volatile solvents,[17] makes it hard to employ conventional processing methods such as drop-casting,[18] spin-coating,[19] and rod-coating.[20] As an alternative approach, chemically modified graphene with improved solution dispersibility, for instance graphene oxide with aqueous dispersibility up to more than 5 wt %, is frequently used as a precursor for solution processing.[9,21,22] Unfortunately, intrinsic degradation of the structures and material properties of graphene is hard to avoid during the chemical modification and subsequent reduction.

In this work, we demonstrate unusually fast interfacial assembly of pristine graphene platelets as a cost-effective and high-yield route to large-area graphene based films. We find

Received: December 1, 2013
Revised: January 28, 2014
Published: February 13, 2014

   dx.doi.org/10.1021/nl404446f | *Nano Lett.* 2014, 14, 1388−1393

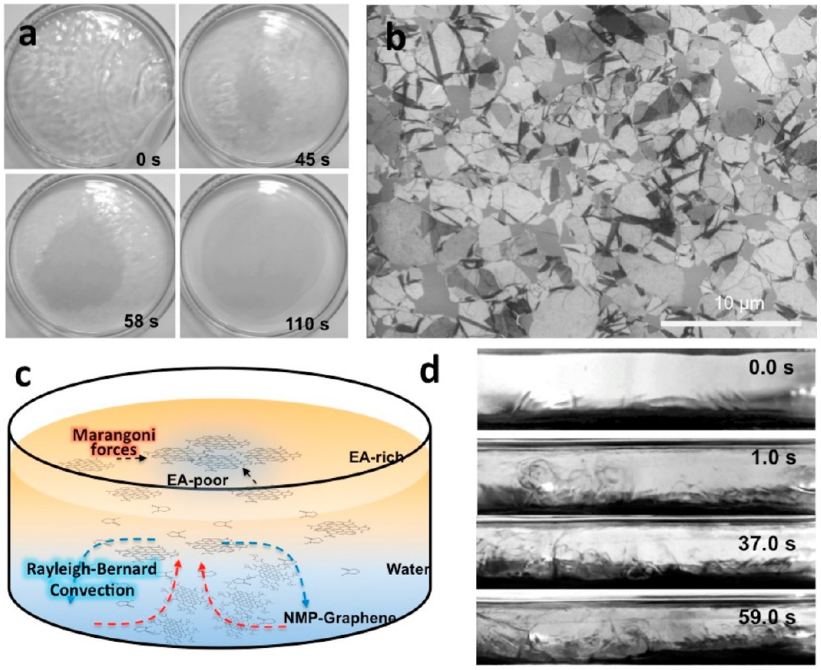

Figure 1. Rayleigh-Bénard convection of pristine graphene platelets toward liquid surface. (a) Time-lapse images of pristine graphene assembly. Graphene platelets are temporarily suspended in water−NMP mixture. EA injection onto the suspension triggers unusually rapid convective transport and assembly of graphene platelets. (b) SEM image of uniform graphene assembled film consisting of closely packed pristine graphene platelets. (c) Schematic illustration of graphene assembly. Graphene platelets are quickly elevated by Rayleigh-Bénard convection and assemble at liquid surface by Marangoni forces. (d) Side-view images of Rayleigh-Bénard convection flow after EA injection.

that pristine graphene platelets temporarily suspended in aqueous media assemble into an arbitrarily large area uniform graphene based film in a few minutes by adding ethyl acetate (EA) to the suspension. This interfacial assembly protocol is applicable other pristine graphitic carbons, including 0D fullerene and 1D carbon nanotubes, that commonly suffer from limited solution compatibility. We systematically investigate the underlying mechanism of this surprising film preparation principle.

The interfacial assembly of graphene platelets is demonstrated in the time-lapse images of Figure 1a (see Supporting Movie S1 in real time). When EA is introduced into a dilute suspension of graphene in an aqueous medium, graphene assembly is typically completed within 2 min over circular area of a 8 cm diameter. Figure 1b shows a typical scanning electron microscopy (SEM) image of the assembled film, where a few layers of pristine graphene platelets are closely packed to form a uniform film. This ultrafast assembly is composed of two distinct steps (Figure 1c): (i) spontaneous migration of graphene platelets toward the liquid surface, and (ii) lateral assembly into a graphene based film. First, we prepare high-quality graphene platelets with different sizes as starting materials for interfacial assembly. Typically, 2−3 layer thick, 1−5 μm diameter microplatelets are prepared by electrochemical exfoliation of highly ordered pyrolytic graphite (HOPG).[23] The 1−3 layer thick, 100−200 nm diameter nanoplatelets are purchased from NanoIntegris, USA (see Supporting Figure S1). Those pristine graphene platelets are suspended in NMP (*N*-methyl-2-pyrrolidone) (0.05 mg/mL) by mild stirring. The resultant pristine graphene suspension is mixed with deionized (DI) water, where the graphene suspension is temporarily stabilized for several minutes due to the solvation of graphene with NMP molecules. If this suspension is maintained for more than a few minutes, the NMP molecules gradually unbind from the graphene surface. causing the aggregation and precipitation of graphene flakes.[24] By contrast, if EA is added before destabilization occurs, graphene platelets rapidly migrate to the liquid surface and assemble into a highly uniform film.

The spontaneous migration of graphene platelets toward the liquid surface is attributed to Rayleigh-Bénard convection[25] caused by evaporative cooling of the EA layer (Figure 1d). EA is partially soluble in water (6−8% v/v). When an excess of EA (approximately 10% v/v) is added into the water−NMP suspension, it forms a thin liquid layer on top of the aqueous media surface. Subsequently, the temperature difference of the top EA layer from underlying aqueous media, caused by the rapid evaporation of volatile EA, induces convection due to a Rayleigh-Bénard instability (see Supporting Movie S2 in real time). In our experimental system, the temperature difference ΔT_h is about 2 °C, as measured by infrared imaging, and the height of aqueous phase h is 20 mm. Under these conditions, we estimate the Rayleigh number R_a using the equation[26]

$$R_a = \frac{g\alpha\Delta T_h}{\eta\kappa}h^3$$

where g is the gravitational acceleration, and the aqueous phase is characterized by its thermal expansion coefficient α, viscosity η, and thermal diffusivity κ. Using $\alpha = 6.9 \times 10^{-5}$ C^{1-}, $\eta = 0.001$ Pa·s, and $\kappa = 3.34 \times 10^{-10}$ m^2/s, the values for water, together with h = 20 mm and ΔT_h = 2 °C, we estimate the Rayleigh number R_a to be 7.5×10^4, far in excess of the critical value of 1100.65.[27] Indeed, direct infrared imaging reveals that convective plumes develop as the top EA/water layer cools (see Supporting Movie S3). This convective flow continually lifts graphene off the bottom surface and brings it to the liquid surface. Obviously, the high vapor pressure of EA is essential for

dx.doi.org/10.1021/nl404446f | *Nano Lett.* 2014, 14, 1388−1393

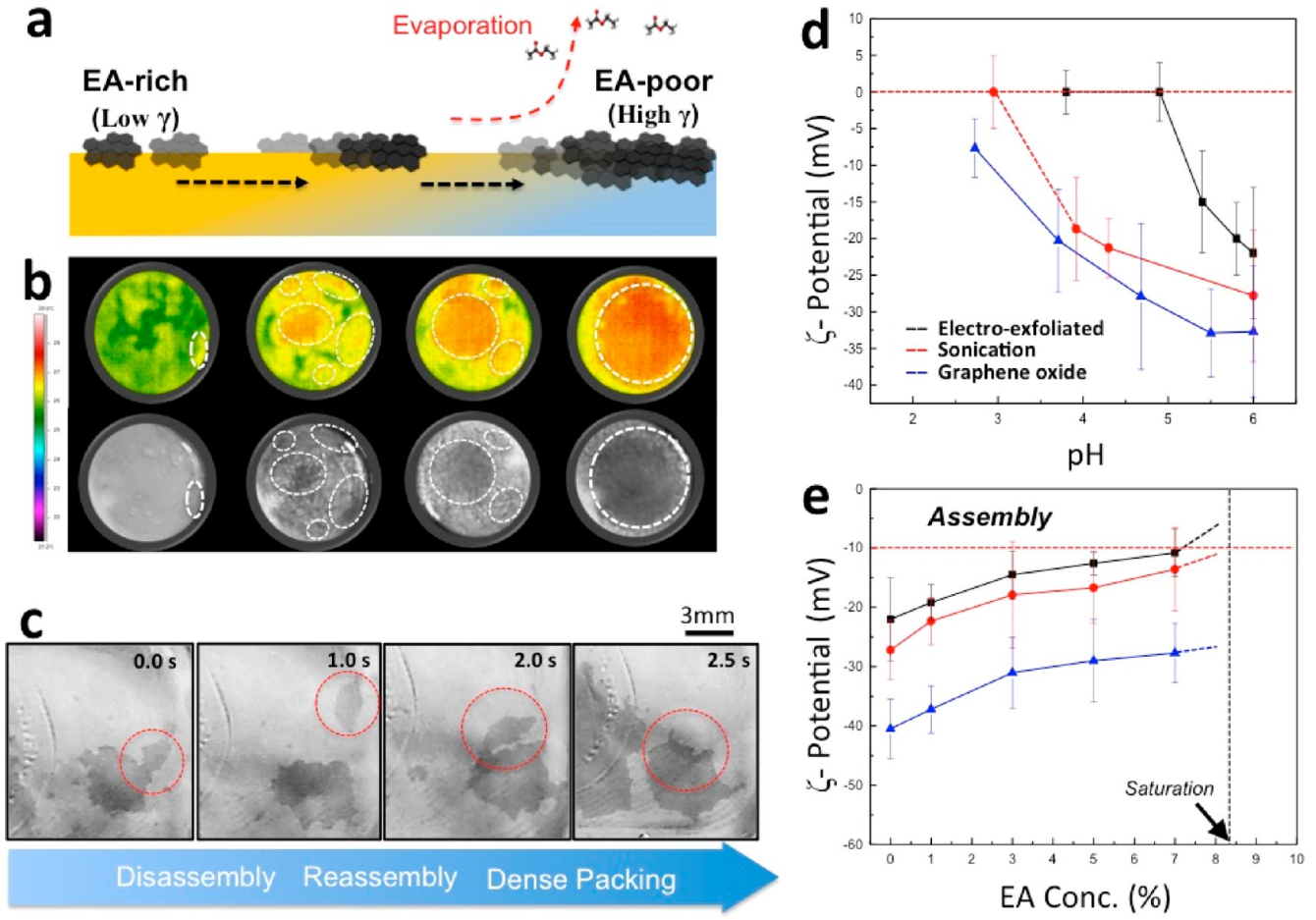

Figure 2. Evaporation induced Marangoni flow for large-scale graphene assembly. (a) Schematic illustration of lateral transport and assembly of graphene platelets. Platelets are transported from lower surface tension region (EA-rich region) to higher surface tension region (EA-rich region), as EA evaporates. (b) Infrared images of liquid surface after EA loading onto the liquid surface. The temperature at the EA-poor regions was lower than EA-rich regions due to the endothermic evaporation. (c) Disassembly and reassembly of graphene platelets to form a tightly packed large-area film. (d–e) Either low pH or EA addition reduces the surface negative charge of graphene platelets in the water–NMP mixture. According to the preparation method of graphene suspension, different surface charge states of graphene platelets are measured.

graphene transport to the liquid surface. Among various tested solvents, only EA and diethyl ether (DEE) could generate strong convective flow at ambient conditions (see Supporting Figure S2).

Another requirement for fast graphene assembly is rapid lateral assembly of the graphene platelets at the liquid surface. If two immiscible or partially miscible liquid phases with surface-active materials lose their equilibrium partitioning, interfacial instabilities can occur.[27] Such instability can be activated by chemical reaction, evaporation, or dilatation/compression at an interface,[28,29] which leads to Marangoni forces parallel to the interface. Marangoni forces have been used for interfacial assembly of colloidal nanoparticles and uniform colloidal films.[30,31] In our system, the distribution of EA at the liquid surface becomes inhomogeneous as the highly volatile EA evaporates. This generates a surface tension gradient induced instability. Graphene platelets move from low surface tension regions (EA-rich) to high surface tension regions (water-rich) at the liquid surface (Figure 2a). Figure 2b shows the inhomogeneous distribution of EA, visualized by infrared imaging (Supporting Figure S3). Because of endothermic evaporation, EA-rich regions exhibit lower temperatures than EA-poor regions. Graphene platelets assemble as soon as they arrive at liquid surface by convention. Growing films are principally observed at EA-poor high surface tension regions. Platelets collide, overlap, and eventually bind to each other via strong $\pi-\pi$ interactions.[32−34] During this lateral assembly, assembled graphene seeds or flakes are continuously perturbed by the surface-tension-driven instability. Interestingly, weakly bound flakes disassemble and reassemble until they are bound strongly enough to withstand the surface flow instability (Figure 2c). The final macroscopic shape of the graphene assembled film is determined by the shape of the container. Significantly, the graphene transport toward the liquid surface and subsequent lateral assembly do not occur serially but coincidently. Such graphene assembly continues until EA on the surface is completely exhausted. Upon further addition of EA, the remaining graphene platelets in the water-NMP suspension can be extracted and assembled into an arbitrarily large area film.

We have performed a control test using DEE as an assembly solvent instead of EA. DEE has a similar water solubility as EA and its vapor pressure and surface tension are sufficiently high and low enough to produce a significant Marangoni force (Supporting Figure S2). Indeed, when DEE is added to the graphene suspension in the water–NMP mixture, graphene platelets rapidly migrate toward the top surface due to Raleigh-Bénard convection, just as for EA. However, active lateral

dx.doi.org/10.1021/nl404446f | Nano Lett. 2014, 14, 1388−1393

assembly does not occur. Only a small number of tiny pieces of graphene assembled films are generated. This difference in behavior between EA and DEE is attributed to their different ionization behavior in water. The edges of pristine graphene platelets prepared from graphite are decorated with negative charged functional groups such as carboxylate.[35−37] While ionic dissociable EA can screen the surface charges, nonionizable DEE does not. The electrostatic repulsion caused by charged edge hinders the lateral assembly of graphene platelets. Figure 2d and 2e compare the surface charge states of the pristine graphene platelets prepared by sonication of graphite in NMP or by electrochemical exfoliation of HOPG and graphene oxide as a function of pH and EA concentration (Supporting Figure S4). Acidity can also suppress the surface charge via deprotonation of carboxylic acid. Even graphene oxide with strong negative charges could be assembled if we added a sufficient quantity of strong acid to the water before adding EA.[38]

An important advantage of our graphene assembly is the tunability of the film morphology and corresponding optical transmittance and electrical conductivity. In particular, the evaporation rate of EA is a critical parameter for determining the film thickness. The evaporation rate is readily controlled using the evaporation chamber, as illustrated in Figure 3a. As the EA composition in the chamber increases (or the evaporation rate of EA decreases), the assembly speed of the graphene based film gradually slows down, and the film thickness increases. Figure 3c shows that the sheet resistance of air-dried graphene assembled film decreases down to 1 kΩ/□ with film thickness. In situ Au doping during graphene interfacial assembly may further reduce the sheet resistance down to 850 Ω/□. Interestingly, when the assembly speed is substantially lowered, the lateral packing of graphene platelets is loosened (Figure 3b). While close packed graphene based films can be used for surface coating or flexible electrodes, such porous films are useful for separation membrane, chemical sensors, and energy storage applications.[15,16] The thickness of graphene assembled film was directly measured by AFM. The typical thickness of the films prepared at ambient condition was about 1.0 nm, which corresponds to approximately three graphene layer stacking (3 × 0.335 nm). This value was also confirmed by the optical transmittance measurement. The optical transmittances at various positions of films were measured by UV−vis spectrophotometry. The average transmittance at 550 nm was about 93%. Using the optical absorbance of 2.3% for monolayer graphene, this value corresponds to three graphene layers stacking, consistent with the AFM measurements. The graphene assembled films can be subsequently stacked into multilayers to control the electrical conductivity and optical transmittance over a broad range (Supporting Figure S5).

The graphene assembled films formed at the liquid surface are readily transferrable to various substrates, including flexible and nonplanar substrates, without any requirement for metal catalyst etching nor polymer residue removal. Figure 4a shows a very large graphene film that has been transferred onto a glass wafer 4-in. in diameter. The optical homogeneity of the transferred film confirms the uniformity of film preparation and transfer. Figure 4b shows that our graphene assembled films can also be transferred to flexible polymer substrates. After transfer, residual solvent can be removed by moderate drying at 195 °C for about 30 min. This method of deposition can also

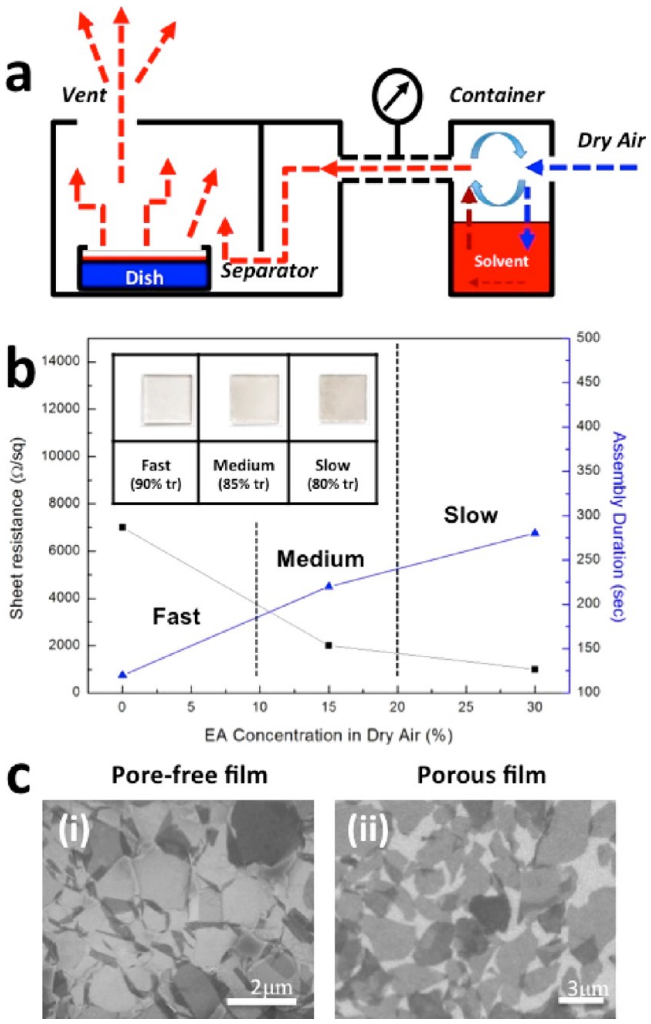

Figure 3. Morphology control of pristine graphene assembled film. (a) Schematic illustration of evaporation control chamber. The amount of EA in the flowing gas stream controls the EA evaporation rate, which subsequently modifies the morphology of graphene film. (b) Relationship among EA content in the gas stream and assembly speed and film sheet resistance. (c) Surface morphology of graphene film measured by SEM. Film morphologies formed at (i) fast evaporation (0% EA in flowing gas) and (ii) slow evaporation (30% EA in dry air), respectively.

generate conductive coatings on silicone beads and other nonplanar surfaces (Figure 4c and Supporting Figure S6).

Significantly, this interfacial assembly is generally useful for the preparation of films from other nanomaterials. For instance, we can generate large-size uniform films of other graphitic carbons including, as representative examples, carbon nanotubes (CNTs) and fullerene. Those 0D and 1D carbon materials are also known to have limited solution compatibility.[39,40] Figure 4d and e shows SEM images of films assembled from single-wall nanotubes (SWCNTs) and multiwall nanotubes (MWCNTs). The assembled morphology of SWCNTs, with their low bending rigidity, shows the morphological trace of lateral packing during interfacial assembly, whereas MWCNTs, which are highly rigid, show a randomized network. As shown in Figure 4f, electron diffraction pattern of fullerene-assembled film demonstrates weak two-dimensional hexagonal packing.

dx.doi.org/10.1021/nl404446f | Nano Lett. 2014, 14, 1388−1393

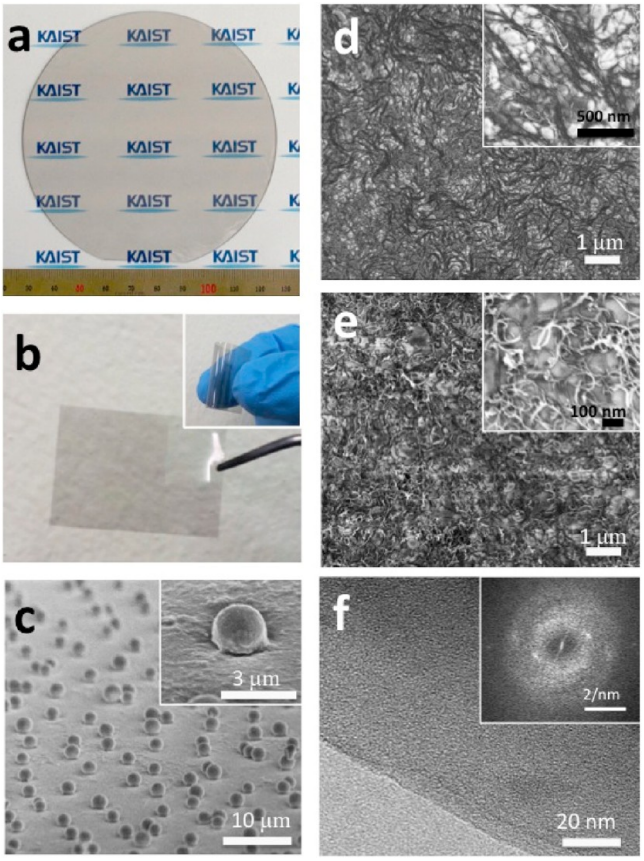

Figure 4. Universal assembly and transfer of graphitic carbons. (a) Graphene film transferred onto 4-in. glass wafer. (b) Graphene film transferred onto flexible poly(ethylene terephthalate) (PET) film. (c) Graphene film covered onto nonplanar surface consisting of silicone particles (2.5 μm diameter) deposited on polydimethylsiloxane (PDMS) substrate. (d) SEM images of single-wall carbon nanotube (SWCNT) assembled film. (e) SEM images of multiwalled carbon nanotube (MWCNT) assembled film. (f) Transmission electron microscopy (TEM) and electron diffraction images of fullerene assembled film. The *d*-spacing of hexagonal fullerene packing is approximately 0.83 nm (inset).

In summary, a surprisingly rapid interfacial assembly of pristine graphene films has been demonstrated. A single shot of volatile solvent into a dilute aqueous suspension of pristine graphene produces a large-area graphene assembled film. Significantly, this assembly principle generally works for various low dimensional nanomaterials, including fullerene and CNTs. Moreover, various in-plane hybrid or composite structures, such as CNT/graphene hybrid lateral assembly, polymer/graphene composites, and metal particles deposited between graphene platelet films, can be straightforwardly assembled by a single-step process (Supporting Figure S7). This facile interfacial assembly with compositional and morphological diversity will greatly broaden the potential of low dimensional nanomaterials for electronics, optoelectronics, and energy/environmental applications.

■ ASSOCIATED CONTENT

Ⓢ Supporting Information

Methods, movies, additional SEM and TEM images, and additional measurements. This material is available free of charge via the Internet at http://pubs.acs.org.

■ AUTHOR INFORMATION

Corresponding Authors

*E-mail: yigira@skkku.edu.
*E-mail: pine@nyu.edu.
*E-mail: sangouk.kim@kaist.ac.kr. Phone: +82-42-350-3339. Fax: +82-42-350-3310.

Author Contributions

S.O.K., J.W.S., and G.-R.Y. designed the original research approach; J.W.S. principally performed graphene assembly and characterization; J.-M.Y. and T.Y. assisted graphene suspension preparation; K.E.L., T.Y.Y., and W.J.L. assisted film characterization; D.J.P., R.R., and P.K. assisted the analysis of graphene assembly. J.S., G.-R.Y., D.J.P., and S.O.K. wrote the manuscript. All authors discussed the experiments and commented on the manuscript.

Notes

The authors declare no competing financial interest.

■ ACKNOWLEDGMENTS

This work is principally supported by the Institute for Basic Science (IBS) (CA-1201-02). G.-R.Y. acknowledges the support from the Korean NRF (grant 2010-0029409). D.J.P. acknowledges the support from the US National Science Foundation (DMR-1105455). P.K. acknowledges the support from the Korean NRF (NRF-2011-35B-D00013).

■ REFERENCES

(1) Geim, A. K.; Novoselov, K. S. The rise of graphene. *Nat. Mater.* **2007**, *6*, 183−191.

(2) Dikin, D. A.; Stankovich, S.; Zimney, E. J.; Piner, R. D.; Dommett, G. H. B.; Evmenenko, G.; Nguyen, S. T.; Ruoff, R. S. Preparation and characterization of graphene oxide paper. *Nature* **2007**, *448*, 457−460.

(3) Hwang, J. O.; Park, S. J.; Choi, D. S.; Kim, J. Y.; Lee, S. H.; Lee, K. E.; Kim, Y. H.; Song, M. H.; Yoo, S.; Kim, S. O. Workfuction tunable, N-doped reduced graphene transparent electrodes for high performance polymer light emitting diodes. *ACS Nano* **2012**, *6*, 159−167.

(4) Li, X.; Cai, W.; An, J.; Kim, S.; Nah, J.; Yang, D.; Piner, R.; Velamakanni, A.; Jung, I.; Tutuc, E.; Banerjee, S. K.; Colombo, L.; Ruoff, R. S. Large-area synthesis of high-quality and uniform graphene films on copper foils. *Science* **2009**, *324*, 1312−1314.

(5) Bae, S.; Kim, H.; Lee, Y.; Xu, X.; Park, J.-S.; Zheng, Y.; Balakrishnan, J.; Lei, T.; Kim, H. R.; Song, Y. I.; Kim, Y.-J.; Kim, K. S.; Ozyilmaz, B.; Ahn, J. H.; Hong, B. H.; Iijima, S. Roll-to-roll production of 30-in. graphene films for transparent electrodes. *Nat. Nanotechnol.* **2010**, *5*, 574−578.

(6) Suk, J. W.; Kitt, A.; Magnuson, C. W.; Hao, Y.; Ahmed, S.; An, J.; Swan, A. K.; Goldberg, B. B.; Ruoff, R. S. Transfer of CVD-Grown Monolayer Graphene onto Arbitrary Substrates. *ACS Nano* **2011**, *5*, 6916−6924.

(7) Rafiee, J.; Mi, X.; Gullapalli, H.; Thomas, A. V.; Yavari, F.; Shi, Y.; Ajayan, P. M.; Koratkar, N. A. Wetting transparency of graphene. *Nat. Mater.* **2012**, *11*, 217−222.

(8) Kim, B. H.; Kim, J. Y.; Jeong, S.-J.; Hwang, J. O.; Lee, D. H.; Shin, D. O.; Choi, S. Y.; Kim, S. O. Surface energy modification by spin cast, large area graphene film for block copolymer lithography. *ACS Nano* **2010**, *4*, 5464−5470.

(9) Stankovich, S.; Dikin, D. A.; Dommett, G. H. B.; Kohlhaas, K. M.; Zimney, E. J.; Stach, E. A.; Piner, R. D.; Nguyen, S. T.; Ruoff, R. S. Graphene-based composite materials. *Nature* **2006**, *442*, 282−286.

(10) Maiti, U. N.; Lim, J.; Lee, K. E.; Lee, W. J.; Kim, S. O. Three-dimensional shape engineered, interfacial gelation of reduced graphene oxide for high rate, large capacity supercapacitors. *Adv. Mater.* **2014**, *26*, 615−619.

(11) El-Kady, M. F.; Strong, V.; Dubin, S.; Kaner, R. B. Laser scribing of high-performance and flexible graphene-based electrochemical capacitors. *Science* **2012**, *335*, 1326−1330.
(12) Gao, W.; Singh, N.; Song, L.; Liu, Z.; Reddy, A. L. M.; Ci, L.; Vajtai, L.; Zhang, Q.; Wei, B.; Ajayan, P. M. Direct laser writing of micro-supercapacitors on hydrated graphite oxide films. *Nat. Nanotechnol.* **2011**, *6*, 496−500.
(13) Schedin, F.; Geim, A. K.; Morozov, S. V.; Hill, E. W.; Blake, P.; Katsnelson, M. I.; Novoselov, K. S. Detection of individual gas molecules adsorbed on graphene. *Nat. Mater.* **2007**, *6*, 652−655.
(14) Han, T. H.; Huang, Y. K.; Tan, A. T. L.; Dravid, V. P.; Huang, J. Steam Etched Porous Graphene Oxide Network for Chemical Sensing. *J. Am. Chem. Soc.* **2011**, *133*, 15264−15267.
(15) Bunch, J. S.; Zande, A. M.; Verbridge, S. S.; Frank, I. W.; Tanenbaum, D. M.; Parpia, J. M.; Craighead, H. G.; McEuen, P. L. Electromechanical resonators from graphene sheets. *Science* **2007**, *315*, 490−493.
(16) Kim, H. W; Yoon, H. W.; Yoon, S. M.; Yoo, B. M.; Ahn, B. K.; Cho, Y. H.; Shin, H. J.; Yang, H.; Paik, U.; Kwon, S.; Choi, J. Y.; Park, H. B. Selective gas transport through few-layered graphene and graphene oxide membranes. *Science* **2013**, *342*, 91−95.
(17) Nuvoli, D.; Valentini, L.; Alzari, V.; Scognamillo, S.; Bon, S. B.; Piccinini, M.; Illescasd, J.; Mariani, A. High concentration few-layer graphene sheets obtained by liquid phase exfoliation of graphite in ionic liquid. *J. Mater. Chem.* **2011**, *21*, 3428−3431.
(18) Li, D.; Muller, M.; Gilje, S.; Kaner, R. Processable aqueous dispersions of graphene nanosheets. *Nat. Nanotechnol.* **2008**, *3*, 101−105.
(19) Yamaguchi, H.; Eda, G.; Mattevi, C.; Kim, H.; Chhowalla, M. Highly uniform 300 mm wafer-scale deposition of single and multilayered chemically derived graphene thin films. *ACS Nano* **2010**, *4*, 524−528.
(20) Wang, J.; Liang, M.; Fang, Y.; Qiu, T.; Zhang, J.; Zhi, L. Rod-coating: Towards large-area fabrication of uniform reduced graphene oxide films for flexible touch screens. *Adv. Mater.* **2012**, *24*, 2874−2878.
(21) Eda, G.; Fanchini, G.; Chhowalla, M. Large-area ultrathin films of reduced graphene oxide as a transparent and flexible electronic material. *Nat. Nanotechnol.* **2008**, *3*, 270−274 (2008).
(22) Cote, L. J.; Kim, F.; Huang, J. Langmuir-Blodgett assembly of graphene oxide single layers. *J. Am. Chem. Soc.* **2009**, *131*, 1043−1049.
(23) Su, C. Y.; Lu, A. U.; Xu, Y.; Chen, F. R.; Khlobystov, A. N.; Li, L. J. High-Quality Thin Graphene Films from Fast Electrochemical Exfoliation. *ACS Nano* **2011**, *5*, 2332−2339.
(24) Hernandez, Y.; Nicolosi, V.; Lotya, M.; Blighe, F. M.; Sun, Z.; De, S.; McGovern, I. T.; Holland, B.; Byrne, M.; Gun'Ko, Y. K.; Boland, J. J.; Niraj, P.; Duesberg, G.; Krishnamurthy, S.; Goodhue, R.; Hutchison, J.; Scardaci, V.; Ferrari, A. C.; Coleman, J. N. High-yield production of graphene by liquid-phase exfoliation of graphite. *Nat. Nanotechnol.* **2008**, *3*, 563−568.
(25) Shih, C.-J.; Lin, S.; Strano, M. S.; Blankschtein, D. Understanding the stabilization of liquid-phase-exfoliated graphene in polar solvents: Molecular dynamics simulations and kinetic theory of colloid aggregation. *J. Am. Chem. Soc.* **2010**, *132*, 14638−14648.
(26) Doumenc, F.; Boeck, T.; Guerrier, B.; Rossi, M. Transient Rayleigh-Bénard-Marangoni convection due to evaporation: A linear non-normal stability analysis. *J. Fluid Mech.* **2010**, *648*, 521−539.
(27) Chandrasekhar, S. *Hydrodynamic and Hydromagnetic Stability*; International Series of Monographs on Physics; Oxford University Press: New York, 1961; pp 212−217.
(28) Sano, O. *Formation and transitions of patterns in thermal convection*; Research of Pattern Formation; KTK Scientific Publishers: Tokyo, 1994; pp 265−288.
(29) Bekki, S.; Vignes-Adler, M.; Nakache, E.; Adler, P. Solutal Marangoni effect: I. pure interfacial transfer. *J. Colloid Interface Sci.* **1990**, *140*, 492−506.
(30) Huang, J.; Kim, F.; Tao, A. R.; Connor, S.; Yang, P. Spontaneous formation of nanoparticle stripe patterns through dewetting. *Nat. Mater.* **2005**, *4*, 896−900.
(31) Fanton, X.; Cazabat, A. M. Spreading and instabilities induced by a solutal Marangoni effect. *Langmuir* **1998**, *14*, 2554−2561.
(32) Xia, Y.; Nguyen, T. D.; Yang, M.; Lee, B.; Santos, A.; Podsiadlo, P.; Tang, A.; Glotzer, S. C.; Kotov, N. A. Self-assembly of self-limiting monodisperse supraparticles from polydisperse nanoparticles. *Nat. Nanotechnol.* **2011**, *6*, 580−587.
(33) Luo, J.; Jang, H. D.; Sun, T.; Xiao, L.; He, Z.; Katsoulidis, A. P.; Kanatzidis, M. G.; Gibson, J. M.; Huang, J. Compression and Aggregation-Resistant Particles of Crumpled Soft Sheets. *ACS Nano* **2011**, *5*, 8943−8949.
(34) W, L.; Chen, F.; Wang, H.; Zeng, T. H.; Wang, Q.; Chen, Y. Acetone-induced graphene oxide film formation at the water-air interface. *Chem. Asian J.* **2013**, *8*, 437−443.
(35) Schniepp, H. C.; Li, J. L.; McAllister, M. J.; Sai, H.; Alonso, M. H.; Adamson, D. H.; Prud'homme, R. K.; Car, R.; Saville, D. A.; Aksay, I. A. Functionalized single graphene sheets derived from splitting graphite oxide. *J. Phys. Chem. B* **2006**, *110*, 8535−8539.
(36) Kim, J.; Cote, L. J.; Kim, F.; Yuan, W.; Shull, K. R.; Huang, J. Graphene Oxide Sheets at Interfaces. *J. Am. Chem. Soc.* **2010**, *132*, 8180−8186.
(37) Reincke, F.; Kegel, W. K.; Zhang, H.; Nolte, M.; Wang, D.; Vanmaekelbergh, D.; Möhwald, H. Understanding the self-assembly of charged nanoparticles at the water/oil interface. *Phys. Chem. Chem. Phys.* **2006**, *8*, 3828.
(38) Lee, S. H.; Lee, D. H.; Lee, W. J.; Kim, S. O. Tailored assembly of carbon nanotubes and graphene. *Adv. Funct. Mater.* **2011**, *21*, 1338.
(39) Maiti, U. N.; Lee, W. J.; Lee, J. M.; Oh, Y.; Kim, J. Y.; Kim, J. E.; Shim, J.; Han, T. H.; Kim, S. O. 25th anniversary article: chemically modified/doped carbon nanotubes & graphene for optimized nanostructures & nanodevices. *Adv. Mater.* **2014**, *26*, 40−67.
(40) Bergin, S. D.; Nicolosi, V.; Streich, P. V.; Giordani, S.; Sun, Z.; Windle, A. H.; Ryan, P.; Niraj, N. P. P.; Wang, Z. T. T.; Carpenter, L.; Blau, W. J.; Boland, J. J.; Hamilton, J. P.; Coleman, J. N. Towards Solutions of Single-Walled Carbon Nanotubes in Common Solvents. *Adv. Mater.* **2008**, *20*, 1876−1881.